

# Biocalcite, a multifunctional inorganic polymer: Building block for calcareous sponge spicules and bioseed for the synthesis of calcium phosphate-based bone

Xiaohong Wang\*, Heinz C. Schröder and Werner E. G. Müller

## Review

Open Access

Address:  
ERC Advanced Investigator Grant Research Group at Institute for  
Physiological Chemistry, University Medical Center of the Johannes  
Gutenberg University Mainz, Duesbergweg 6, D-55128 Mainz,  
Germany

Email:  
Xiaohong Wang\* - wang013@uni-mainz.de

\* Corresponding author

Keywords:  
biocalcite; bioprinting; bone; bone formation; calcareous spicules;  
sponge

*Beilstein J. Nanotechnol.* **2014**, *5*, 610–621.  
doi:10.3762/bjnano.5.72

Received: 10 January 2014  
Accepted: 16 April 2014  
Published: 12 May 2014

Associate Editor: C. Steinem

© 2014 Wang et al; licensee Beilstein-Institut.  
License and terms: see end of document.

## Abstract

Calcium carbonate is the material that builds up the spicules of the calcareous sponges. Recent results revealed that the calcium carbonate/biocalcite-based spicular skeleton of these animals is formed through an enzymatic mechanism, such as the skeleton of the siliceous sponges, evolutionarily the oldest animals that consist of biosilica. The enzyme that mediates the calcium carbonate deposition has been identified as a carbonic anhydrase (CA) and has been cloned from the calcareous sponge species *Sycon raphanus*. Calcium carbonate deposits are also found in vertebrate bones besides the main constituent, calcium phosphate/hydroxyapatite (HA). Evidence has been presented that during the initial phase of HA synthesis poorly crystalline carbonated apatite is deposited. Recent data summarized here indicate that during early bone formation calcium carbonate deposits enzymatically formed by CA, act as potential bioseeds for the precipitation of calcium phosphate mineral onto bone-forming osteoblasts. Two different calcium carbonate phases have been found during CA-driven enzymatic calcium carbonate deposition in in vitro assays: calcite crystals and round-shaped vaterite deposits. The CA provides a new target of potential anabolic agents for treatment of bone diseases; a first CA activator stimulating the CA-driven calcium carbonate deposition has been identified. In addition, the CA-driven calcium carbonate crystal formation can be frozen at the vaterite state in the presence of silintaphin-2, an aspartic acid/glutamic acid-rich sponge-specific protein. The discovery that calcium carbonate crystals act as bioseeds in human bone formation may allow the development of novel biomimetic scaffolds for bone tissue engineering. Na-alginate hydrogels, enriched with biosilica, have recently been demonstrated as a suitable matrix to embed bone forming cells for rapid prototyping bioprinting/3D cell printing applications.

## Introduction

The size and complexity of a metazoan taxon is correlated with the dimensioning of its respective complex composite skeleton. This statement can be exemplarily illustrated by comparing different sponge [phylum: Porifera] species. These animals are grouped to the classes of the siliceous sponges, the Hexactinellida and the Demospongia, and the calcareous sponges, the Calcarea [1,2]. Sponges of the “crusty” asconoid type Calcarea, e.g., the encrusting *Clathrina coriacea*, measure about 2 mm in thickness, the syconoid type calcareous sponges, e.g., *Sycon raphanus* have an axis length of 1–5 cm, while species with a leuconoid type Bauplan can be up to 3 m in size, e.g., the demosponge *Sphaciospongia vesparium*, or the hexactinellid *Monorhaphis chuni* [1,2]. The evolutionary oldest animals on earth to comprise a skeleton formed of biosilica and are found among the siliceous sponges, the Hexactinellida and later in the Demospongiae [3,4], while the mineralized skeletons of the calcareous sponges are built of calcite [5]. The selection of the mineral appears to parallel the levels of silicate and carbonate in the marine environment [6].

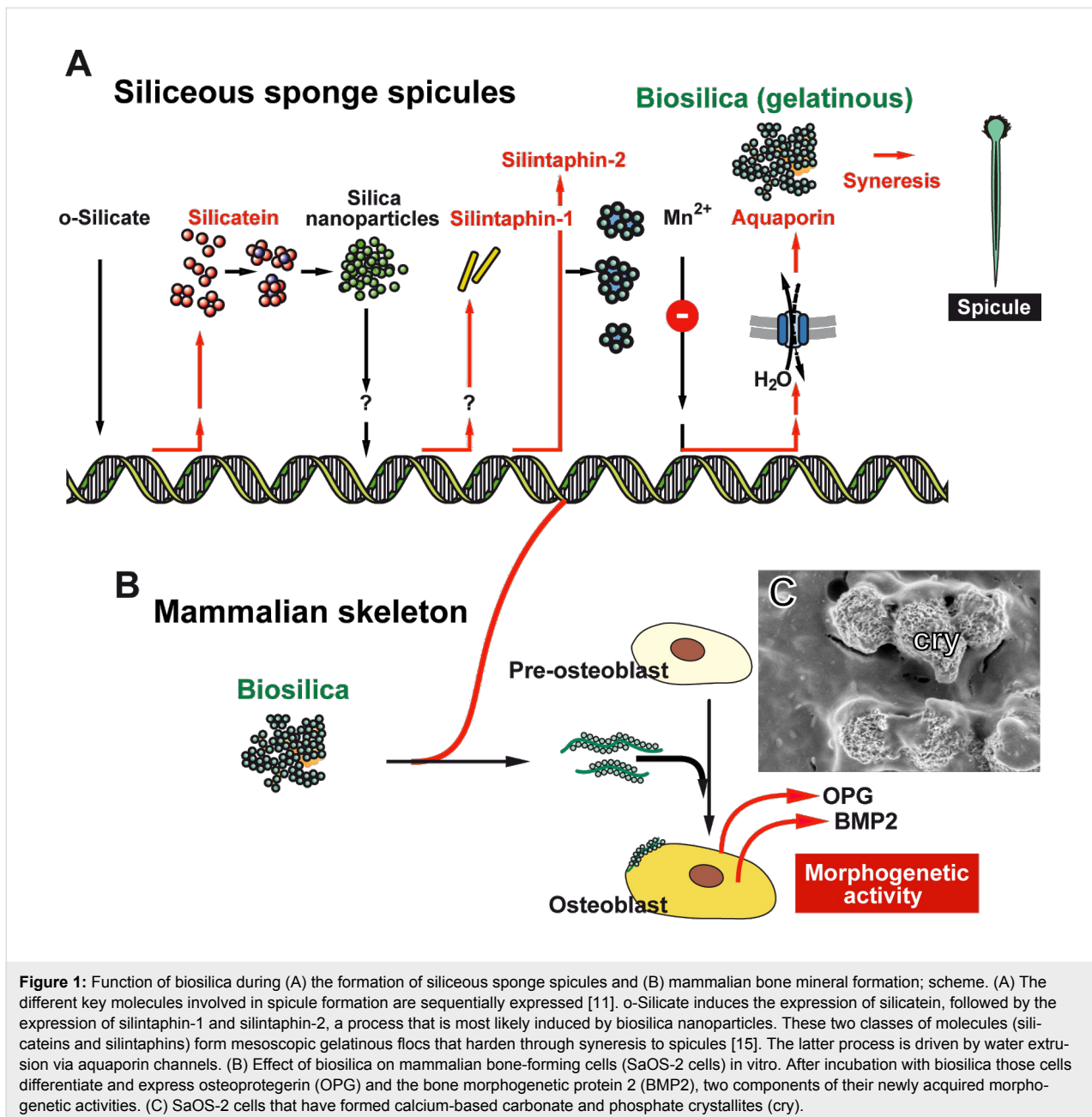
The distinguished feature of biosilica-based skeletons is the fact that this polymer is formed enzymatically, a finding that resulted in the introduction of a new paradigm in biochemistry that also *inorganic polymers* and not only *organic polymers* can be formed enzymatically from their respective precursors [7]. This first clue, together with the finding that all animals, including the sponges, are of monophyletic origin gave the basis for the view that the bodyplan of the metazoans follows more universal genetic blueprints and, in turn, more general biochemical relationships [8].

Following this intellectual approach we asked the question, does the evolutionary oldest inorganic polymer, biosilica, share a functional relationship with the skeletal elements of the crown mammals, the calcium phosphate/hydroxyapatite (HA)-based skeletal systems. The understanding of the genetic blueprint of any morphogenetic event must begin with the identification and functional characterization of the individual expressed genes (proteins), followed by the elucidation of the interaction of the proteins, e.g., acting during mineralization, in other words, should start with the disclosure of the regulatory network of the proteins involved. It should be the aim to unravel the regulatory genetically-controlled architecture of proteins, based on the expression of a few molecules, and to pinpoint a single master gene that, after switching on, initiates the direction of development of a structural skeletal element.

Only recently it was possible to describe the molecular level of the formation of a hard skeleton (reviewed in [4]). Initial investigations were successfully performed with the siliceous

sponge spicules. The key discovery was the identification of silicatein, the enzyme that initiates the biocatalytic biosilica-condensation reaction [9–11]. It initiated the resolution of the biochemical processes leading to biosilica formation (Figure 1A). The silicateins are members of the cathepsin L and papain family of proteases. They have been discovered in the demosponge *Tethya aurantium* by the group of Morse [9,10] and soon thereafter were also identified in the demosponge *Suberites domuncula* [11]. Based on biochemical studies, three isoforms of silicatein have been described in *T. aurantium*, silicatein- $\alpha$  to - $\gamma$ . They have similar molecular weights (approximately 34 kDa). Among them the silicatein- $\alpha$  is the dominant isoform, forming the axial filament, residing in the axial canal. In *T. aurantium* the molar ratio between silicatein- $\alpha$  and silicatein- $\beta$  was determined to be 2:1, while in *S. domuncula* the molar ratio amounts to 4:1. Soon after the expression of the silicateins and after the first formation of silica nanoparticles, the silicatein-interacting proteins, the silintaphins, are read out (Figure 1A). Until now two silintaphins, silintaphin-1 [12] and silintaphin-2 [4], have been described extensively. Silintaphin-1 significantly enhances the biosilica-forming activity of silicatein in vitro. A 5.3-fold increase of the biosilica-forming activity is measured at a molar ratio of 4:1 [silicatein- $\alpha$ /silintaphin-1] [13]. Likewise, in *S. domuncula* the 15-kDa protein silintaphin-2 had been identified as a second silicatein-interactor. Like silintaphin-1, this protein is located in the axial filament, but particularly in the organic cylinder around the growing spicules. Silintaphin-2 is a  $\text{Ca}^{2+}$ -binding protein that complexes four  $\text{Ca}^{2+}$  ions [14].

The formation of HA and HA resorption by osteoclasts and osteoblasts in bone tissue are controlled by a network of cytokines and growth factors. The receptor activator of NF- $\kappa$ B (RANK) and its ligand, receptor activator of NF- $\kappa$ B ligand (RANKL) and osteoprotegerin (OPG) play a key function in regulation of bone formation and bone degradation (reviewed in [16]). The molecular triad OPG/RANKL/RANK not only regulates the differentiation of osteoclasts, but also differentiation processes in the vascular system and in the immune system. Addition of biosilica leads to an increased expression of OPG. The consequence is an inhibition of the differentiation of osteoclasts from their respective precursor cells (Figure 1B). In addition, after exposure of SaOS-2 cells to biosilica these cells increase the synthesis of the bone morphogenetic protein 2 (BMP2), a cytokine that induces osteoblast differentiation and mineralization (Figure 1C) (see [17,18] and reviewed in [16]).



## Review

### Calcium carbonate/bicarbonate a potential bioseed for Ca phosphate mineral formation by osteoblasts

It is well established that the calcium salt of carbonate is an effective diet supplement for amelioration of bone-loss during postmenopausal osteoporosis [19]. Recently, we could show in in vitro studies, by using SaOS-2 cells growing in calcium bicarbonate-deprived medium that these cells respond with a significant increase in calcium deposit formation after exposure to bicarbonate [20]. The cells start to form larger crystallite

nodules on their surfaces, compared to the controls. Of course, the prerequisite has to be fulfilled that simultaneously with bicarbonate the cells have to be treated with the mineralization activation cocktail (MAC), composed of  $\beta$ -glycerophosphate, ascorbic acid and dexamethasone. One plausible explanation that emerged from this observation was that those crystallites, which have been formed metabolically, are composed of calcium carbonate. This assumption was corroborated by the well established finding that mammalian skeletons contain, besides of HA-composed bones, biomineralized otoliths in the vestibular labyrinth of the vertebrate ear. There the inorganic matrix consists to 90 to 95% of calcium carbonate in the arago-

nite form [21,22]. Not only in those skeletal elements but also in the vertebrate bones calcium carbonate co-exists to a considerable amount with Ca phosphate [23].

Under physiological conditions the major processes of biomineralization of bone, teeth and otoconia proceeding in vertebrates mainly occur extracellularly, while intracellular mineral deposits are predominantly assembled during pathological calcifications of soft tissues [24]. Bone formation is based on a tightly controlled process between osteoblasts and fibrillar organic structures that starts from collagen fibrils around which poorly crystalline carbonated apatite aggregates are deposited [25,26]. Carbonated apatite are deposits in which carbonate ions ( $\text{CO}_3^{2-}$ ) reversibly substitute either phosphate ( $\text{PO}_4^{3-}$ ) or hydroxyl ( $\text{OH}^-$ ). Analyses by X-ray and electron diffraction and Fourier transform infrared spectroscopy, as well as determination of the chemical composition revealed that at least under in vitro conditions in osteoblasts low concentrations of carbonate ions exist in their  $\text{Ca}^{2+}$ /phosphate mineral phase. Parallel spectroscopic studies suggested that Ca-deposition in osteoblasts starts intracellularly in calcium-rich vesicles that substantially contribute to the formation of bone apatite [27].

Both calcium phosphate formation [28] and calcium carbonate deposition [29] are exergonic processes that, in turn, are thermodynamically possible, but are strictly controlled in a biochemical system through the activation energy barriers that prevent a chemical reaction from occurring at physiological temperatures/conditions [30]. A modulation of the activation energy barriers enables an organism to control under which physiological conditions a thermodynamically possible reaction can be initiated or prevented [30]. Almost exclusively, alterations of the heights of the activation energy barriers are adjusted by enzymes or by the surface architecture of membranes separating two phases. The recent findings that in animals the inorganic polymer biosilica (see: [4,7]) is synthesized enzymatically through silicatein prompted us to study if also during calcium carbonate deposition there is an enzyme-driven step involved [31].

### Carbonic anhydrase, the basis for the accelerated calcium carbonate synthesis in calcareous sponges

The prevalent enzymes that allow bicarbonate to be formed in an organism are the carbonic anhydrases [CAs] [32]. These enzymes, which are characterized by an extremely high turnover number, catalyze the reversible hydration of carbon dioxide ( $\text{CO}_2$ ) to bicarbonate. This reaction occurs also in the presence of Ca ions [33]. Four of the seven metazoan CA isoenzymes are cytosolic, CA-I, -II, -III, and -VII. Among them the CA-II is a widely studied one [34]. Recently, experimental

evidences have been presented revealing that the CAs might be involved in bone formation [35]. The mammalian CA-II, a cytosolic enzyme, is targeted in intact cell systems under certain physiological conditions to the cell membrane [36,37].

Among the phylogenetically oldest animals that have a skeleton based on calcium carbonate are the calcareous sponges with *Sycon raphanus* as an example (Figure 2A), the CA enzyme was cloned, expressed and functionally tested [38]. From this organism the complete cDNA encoding for the CA was obtained (accession number CCE46072). The complete 1,476 nts cDNA encodes, within its ORF [open reading frame] (from nt<sub>68–70</sub> to nt<sub>1001–1003</sub>), the 312 aa putative CA, having a  $M_r$  of 33,251 and an pI of 5.81. The closest human related CA to the *Sycon* enzyme (Figure 2C), the human CA-X (CAHA\_HUMAN; Q9NS85), and -XI (CAHB\_HUMAN; O75493), are grouped to the "acatalytic" CA isoforms of unknown function, which have been proposed to be devoid of  $\text{CO}_2$  hydration activity [39]. However, the branch with the two sponge CAs comprises a common origin with the stony coral *Stylophora pistillata* enzyme [40] for which an enzymatic activity has been proven. Those human CAes, comprising  $\text{CO}_2$  hydration activity (the catalytic CA), are in the CA group I to IV.

The Zn-binding sites that are involved in the catalytic reaction (hydration of  $\text{CO}_2$ ) are present in the CA-alpha (vertebrate-like) group stretch of the *S. raphanus* protein. The Zn ions are bound to the enzyme through the three His residues in the catalytic center of the enzyme [41]. The presence of a signal peptide cleavage site in the sponge CA indicates that this enzyme is secreted by the sponge cells or bound to the cell membrane. The spicules from the calcareous sponges (Figure 2B), e.g., *Sycon* used in our studies [38,42], consists of almost pure calcium carbonate (calcite). In a first approach to investigate the formation of the calcareous spicules on the molecular level, the function of the CA in this process has been studied by using *S. raphanus* as a model. The cDNA of the *Sycon* CA was prepared in a recombinant way and used to raise antibodies. Immunostuctural studies revealed that the *Sycon* CA is localized on the surface of mature, developed spicules, the ca. 300  $\mu\text{m}$  long diactines and the ca. 300  $\mu\text{m}$  large triactines and tetractines (Figure 3A and B). It is assumed that the membranous, organic sheaths described to cover the spicules [43,44] are composed predominantly of this enzyme. Subsequently the recombinant enzyme was used to determine the in vitro calcium carbonate formation by applying the in vitro diffusion assay [45].

Even though the present-day oceans are supersaturated with respect to calcium carbonate, only very rarely spontaneous abiotic precipitation is seen [46]. Like in other metazoan

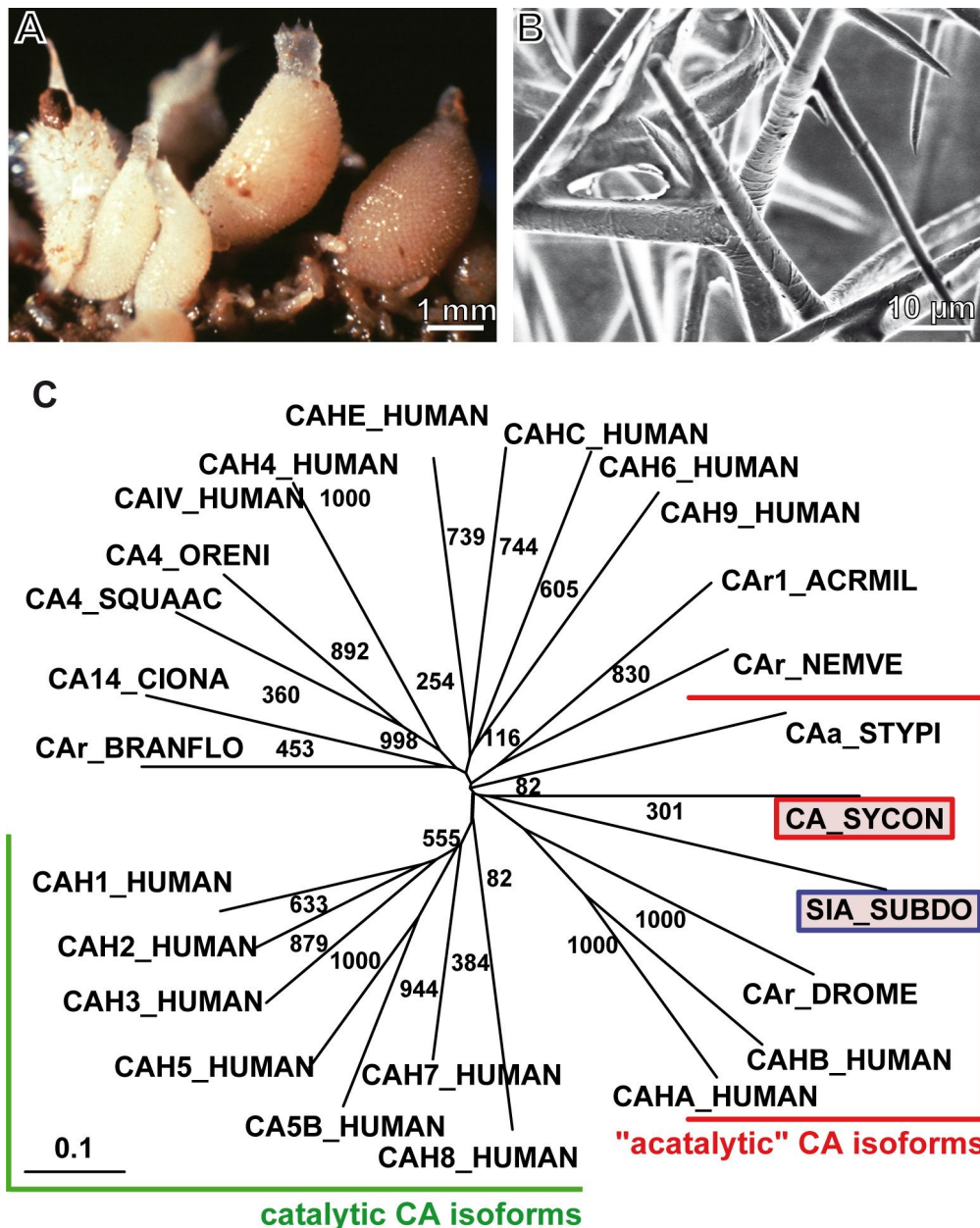


**Figure 2:** *Sycon raphanus*, its spicules and its CA. (A) Specimens of *S. raphanus*; (B) the calcareous spicules. (C) Phylogenetic, radial tree computed with the putative calcareous sponge *S. raphanus* carbonic anhydrase (CA\_SYCON; accession number CCE46072) and the demosponge *S. domuncula* silicase (SIA\_SUBDO; DD298191), as well as the carbonic anhydrase isoforms from human: I (CA-I) (CAH1\_HUMAN; P00915); II (CA-II) (CAH2\_HUMAN; P00918); II-2 (CA II) (CAHB\_HUMAN; O75493), III (CA-III) (CAH3\_HUMAN; P07451); IV (CA-IV) (CAH4\_HUMAN; P22748); VA (CAH5\_HUMAN; P35218); VB (CA5B\_HUMAN; O75493); VI (CA-VI) (CAH6\_HUMAN; P23280); VII (CA-VII) (CAH7\_HUMAN; P43166); VIII (CA-VIII) (CAH8\_HUMAN; P35219); IX (CA-IX) (CAH9\_HUMAN; Q16790); X (CA-RP X) (CAHA\_HUMAN; Q9NS85); XII (CA-XII) (CAHC\_HUMAN; O43570); XIV (CA-XIV) (CAHE\_HUMAN; Q9ULX7). In addition, the related sequences from the scleractinian *Acropora millepora*-1 (CAr1\_ACRMIL; ACJ64662.1), the stony coral *Stylophora pistillata* (CAa\_STYPI; ACA53457.1, EU159467.1), the anthozoan *Nematostella vectensis* (CAr\_NEMVE; XP\_001627923.1), the tunicate *Ciona intestinalis* (CA14\_CIONA; XP\_002123314.1), the lancelet *Branchiostoma floridae* (CAr\_BRANFLO; XP\_002601262.1), the shark *Squalus acanthias* (CA4\_SQUAAC; AAZ03744.1), the fish *Oreochromis niloticus* (CA4\_ORENI; XP\_003456174.1), and the insect enzyme from *Drosophila melanogaster* (CAr\_DROME; NP\_572407.3) are included. The CAs, belonging to the "acatalytic" CA isoforms and of the catalytic CA isoforms, are surrounded. Partially taken from [38] with permission.

systems, e.g., mollusks or echinoderms, in sponges carbonate is taken up from the aqueous environment as bicarbonate via specific membrane transporters, characterized by a

Michaelis–Menten constant of around 50 mM [47], or is produced metabolically. At this concentration, calcium carbonate precipitates at an extent of about 50% during an incu-

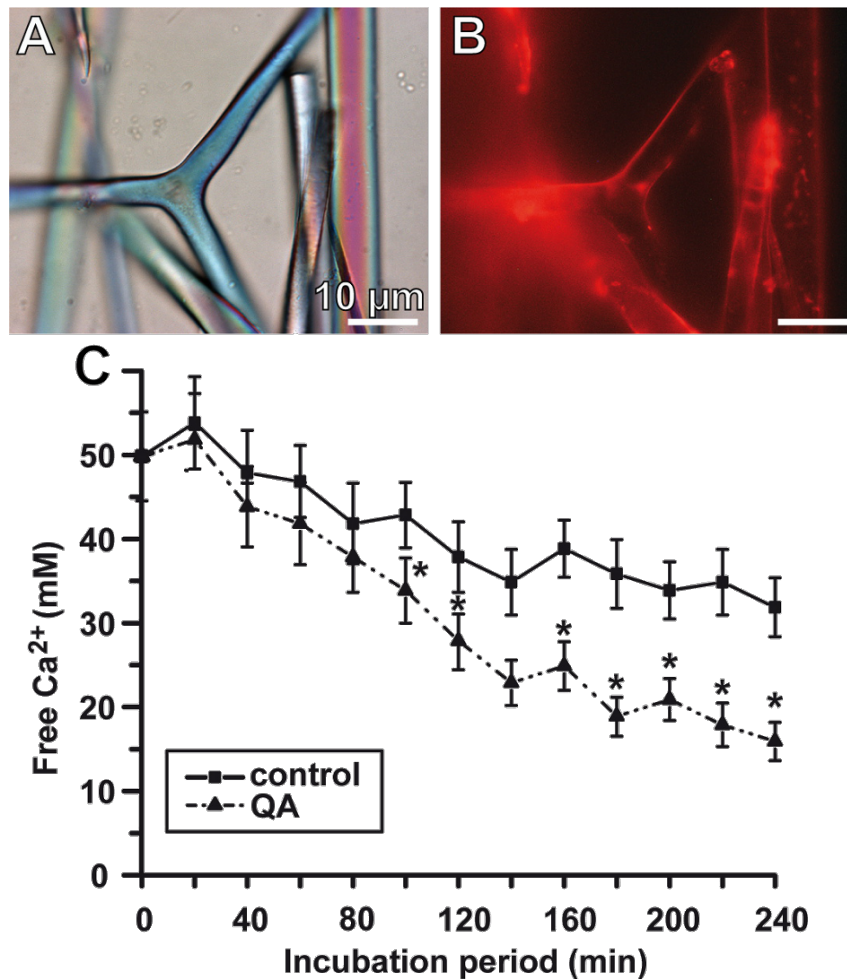


**Figure 3:** *Sycon* CA, its localization and in vitro function. Reacting of *Sycon* spicule with antibodies, raised against the homologous CA. (A) Light microscopic image of the spicules (in the center is a large triactine). (B) The spicules have been reacted with polyclonal antibodies, raised against the *Sycon* CA. The immunocomplexes were stained with Cy5-labelled anti-rabbit IgG. (C) Formation of  $\text{CaCO}_3$  in the ammonium carbonate diffusion assay in the presence of CA. For this series of experiments the recombinant human CA2 enzyme, expressed in *Escherichia coli* (C6624, Sigma), with a specific activity of about 5,000 units/mg, was added at a concentration of 35 W-A units (10  $\mu\text{g}$ )/500  $\mu\text{L}$  of  $\text{CaCl}_2$  to the assays. The formation of calcium carbonate was determined quantitatively on the basis of the consumption of free  $\text{Ca}^{2+}$  ions using the EDTA titration procedure [31]. The assays either remained free of additional compound(s) or were supplemented with 10  $\mu\text{M}$  quinolinic acid (QA, filled triangle). Samples of six parallel determinations were quantitated; means  $\pm$  SD are given. \* $p < 0.05$ .

bation period of only 20 h in an ammonium carbonate diffusion/“dessorator assay” at pH 7–8 [48]. However, this reaction velocity is too slow to account for the rate of calcium carbonate deposition measured in vivo, e.g., in the sponge spicule formation in *Sycon* sp. [49]. The *Sycon* spicules, with a diameter of about 4  $\mu\text{m}$  and a length greater than 100  $\mu\text{m}$ , show a very fast growth rate of 65  $\mu\text{m}/\text{h}$ . Hence it has to be concluded that an acceleration of the velocity of the exergonic reaction at ambient environmental conditions has to occur by lowering the activation energy by an enzyme, or by allowing the calcium carbonate process to proceed on a functionalized organic surface. In our previous studies we tested the first possibility [7,31].

As the substrate for the enzymatic reactions in the “dessorator assay” we used a solution of 50 mM  $\text{CaCl}_2$  over which  $\text{CO}_2$  vapor, generated from  $\text{NH}_4\text{HCO}_3$  solution, was passed. The pH of the reactions was adjusted to 7.5 [7,31]. The mineralization process (based on the decrease of free  $\text{Ca}^{2+}$  concentration measured) started after an initial lag phase of 5 h. Addition of the recombinant CA (35 W-A units/500  $\mu\text{L}$ ) significantly increased the reaction velocity and accelerated the mineralization process; after 50 min already 25% of the  $\text{CaCl}_2$  had been precipitated, in the presence of  $\text{CO}_2$ , to calcium carbonate (Figure 3C). An extent of 80% of precipitated calcium carbonate was reached after 10 h. To highlight again, the major role of the CA during the stages of enzymatic synthesis of

calcium carbonate is to accelerate the reaction velocity, an essential feature of any enzyme. Furthermore, the CA allows the process of calcium carbonate deposition to occur at ambient physiological conditions.

Two morphologically different deposits are formed in the in vitro assay in the presence of the CA (35 W-A CA units per assay): first prisms with an average size of 80–120  $\mu\text{m}$  and second round-shaped deposits of similar dimensions (Figure 4). Predominantly prisms with a rhombohedral morphology are formed, which are composed of calcite, as analyzed by MIDAC Fourier transform infrared spectroscopy (the characteristic vibrational bands at  $873\text{ cm}^{-1}$  and  $711\text{ cm}^{-1}$ ; Figure 4, left crystal). Intermediately, during the formation of the calcite crystals, round-shaped vaterite deposits are formed ( $875\text{ cm}^{-1}$  and  $744\text{ cm}^{-1}$ ; Figure 4, right crystal). It is remarkable and likewise indicative that the biogenic CA-driven calcium carbonate crystal formation can be frozen at the vaterite state (in spite of the overall thermodynamically possible “end-point” transition formation to calcite) if the CA-driven reaction proceeds in the presence of silintaphin-2, a sponge-specific protein that is rich in aspartic acid (Asp, D) and glutamic acid (Glu, E) [50]. The hardness, elastic modulus and creep of the two forms of the calcium carbonate deposits, the calcitic prisms and the round-shaped vaterite deposits were determined by nanoindentation. The load–displacement curves obtained for the two calcium carbonate forms revealed the following values: for the rhombohedral calcite  $1.98 \pm 0.31\text{ GPa}$  and for the round-shaped vaterite deposits only  $1.38 \pm 0.39\text{ GPa}$ . Concurrently, a distinct decrease of the elastic modulus was measured for the vaterite deposits ( $39.13 \pm 8.04\text{ GPa}$ ), in comparison to the rhombohedral calcite prisms ( $72.83 \pm 11.68\text{ GPa}$ ). This significant difference in the mechanical properties between the two morphologies can also be deduced from the creep behavior. While the creep characteristics for the rhombohedral calcitic prisms was found to be

$5.44 \pm 1.15$  (per maximal depth [%]), the corresponding value for the round-shaped vaterite deposits is  $9.95 \pm 1.60$ .

The enzyme-mediated deposition of calcium carbonate is markedly temperature dependent [31]. While at  $10\text{ }^\circ\text{C}$  the reaction velocity of calcium carbonate deposition is almost identical in the enzyme-containing and enzyme-lacking assays, at higher, physiologically more relevant incubation temperatures (e.g.,  $22\text{ }^\circ\text{C}$  [42]), the reaction velocity of the CA-driven calcium carbonate formation is significantly higher (about 2-fold) than that in the absence of CA. Varying the pH value in the precipitation assay shows that in the absence of CA the precipitation of calcium carbonate increases only slightly from pH 6.0 to pH 8.1. In contrast, the CA-driven reaction velocity increases markedly (by over 5-fold) from pH 6.0 to pH 8.0. Importantly, the increased rate in the reaction velocities seen in the CA-containing assays can be inhibited almost completely by the CA-specific inhibitor acetazolamide at  $3\text{ }\mu\text{M}$ . In those assays the calcium concentration had been  $50\text{ mM}$  with respect to  $\text{CaCl}_2$  [31]. These findings are compatible with the view that the calcium carbonate deposition in the system described is enzymatically driven by the CA.

In order to underscore the dominant enzymatic contribution to the calcium carbonate deposition in vitro, one kinetic characteristic, the Michaelis–Menten constant, for CA, was determined [31]. At first it should be mentioned that the reaction follows substrate saturation kinetics. Under the assay conditions used ( $50\text{ mM CaCl}_2$ , pH 7.5,  $25\text{ }^\circ\text{C}$ ), the linear increase of the reaction velocity is seen between 0 and  $20\text{ mM CaCl}_2$ . Only at higher concentrations a saturation level is approached. It is well established that the CAs function both as hydratase, in the formation of bicarbonate, and also as esterase [51]. The Michaelis–Menten constants ( $K_m$ ) for both reactions are almost identical at around  $5\text{ mM}$  for the hydratase (using  $\text{CO}_2$  as substrate) and for the esterase (with the substrate 4-nitrophenylacetate). The constant  $K_m$  for the sponge CA/esterase was determined by applying the method of Lineweaver and Burk. The apparent  $K_m$  constant for the sponge recombinant CA using 4-nitrophenylacetate as esterase substrate was found to be  $6.2 \pm 1.0\text{ mM}$ , at a maximal reaction velocity of  $0.32 \pm 0.05\text{ mmol}\cdot\text{mL}^{-1}\cdot\text{min}^{-1}$ . Using the same approach, the apparent  $K_m$  constant in the hydratase/ $\text{CO}_2$  diffusion assay was calculated to be  $9.9 \pm 2.1\text{ mM}$  (with respect to  $\text{CaCl}_2$ ) at a corresponding  $v_{\text{max}}$  of  $24.9 \pm 3.7\text{ mmol}\cdot\text{mL}^{-1}\cdot\text{min}^{-1}$ .

### Carbonic anhydrase: Evidence for forming bioseeds during mammalian hydroxyapatite formation

Our experimental data show that SaOS-2 cells, exposed to bicarbonate and the MAC, form a significantly increased

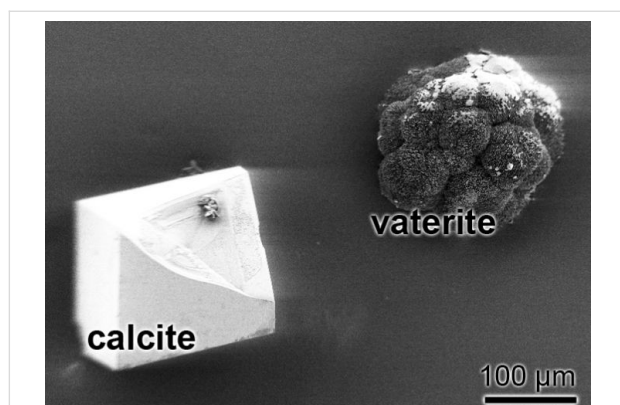


**Figure 4:** Calcium carbonate crystals formed in vitro (ammonium carbonate diffusion assay) by using Sycon CA. Left: a calcite crystal formed; at the right a vaterite crystal that has been formed.

amount of Ca-deposits, as analyzed by a staining procedure with alizarin red S [7]. The MAC supplement (ascorbic acid,  $\beta$ -glycerophosphate and dexamethasone) stimulates cellular differentiation processes. Importantly, it had been measured that this process is paralleled by an enhanced expression of the CA-II gene, suggesting its participation in the Ca-deposit formation. Furthermore, the CA-II inhibitor acetazolamide significantly inhibited the Ca-mineral deposition process. These data favor the assumption that a CA-II-driven enzymatic process is involved in the formation of calcium carbonate bioseeds, required for the initial Ca phosphate deposit synthesis onto SaOS-2 cells. The CA-II is ubiquitously present in the cytoplasm of almost all metazoan cells and, focusing on mammalian bone cells, is probably involved in bone resorption [52]. There, CA-II causes proton production, resulting in a drastic acidification of the resorption lacuna/bone regions. However, recent studies implicate that this enzyme is also involved in bone formation [35]. These surprising Janus-faced catabolic/anabolic metabolic reactions, controlled by CAs might be explained on account of the reversibility of the CA-catalyzed reaction. The CA acts both as a calcium carbonate anabolic enzyme, facilitating and accelerating bicarbonate formation, a precursor molecule for calcium carbonate synthesis, and also as a catabolic enzyme that promotes calcium carbonate dissolution, as shown, e.g., in corals [53]. Experimental data revealed that during the initial phase of the controlled bone-synthesizing process poorly crystalline carbonated apatite is deposited, which contains several percents (4–6 wt %) of carbonate in the apatite crystals [54,55]. Recent studies suggest that the increased carbonate content in apatite crystals has an anabolic effect on bone formation [56]. Our EDX mapping studies [20] indicate that the crystallites initially formed onto SaOS-2 cells are not only rich in the elements calcium and phosphorous but also in carbon. We have taken this observation as a further indication that carbonate and phosphate deposits are co- or sequentially synthesized onto SaOS-2 cells, during the initial phase of mineral formation. Furthermore, the CA-II has been proven to be (under certain physiological conditions [pH regulation]) localized at the plasma membranes of human pancreatic cells [36], where the enzyme is involved both in pH regulation and in the secretion of bicarbonate through the  $\text{Cl}^-/\text{HCO}_3^-$  exchanger [57] and/or an additional  $\text{HCO}_3^-$  channel [36]. We concluded from the data gathered [20] that the calcium phosphate/HA deposition reactions in bone tissue are preceded by calcium carbonate precipitation, a process that is driven by an increased CA activity (Figure 5).

### Carbonic anhydrase: A new target for bone anabolic agents

A number of therapeutic targets have been described influencing signaling pathways, and/or transcription factors to stimu-

late bone growth (see [59]). Among those are the BMP/SMAD, Wnt/ $\beta$ -catenin, Hedgehog/Gli, IGF, and FGF pathways. Emerging evidence indicate that the CA enzyme could also be tackled as a promising target for activators to stimulate calcium carbonate/phosphate mineral deposition onto bone cells. Only very little experimental evidence has been presented that supports our supposition that CA activators exert a potential therapeutic effect on bone anabolism [60]. Until now only a few CA activators have been identified, but none of them have been tested for its potential in the treatment of bone disorders [61–63]. This view might be changed in view of the now available data indicating that calcium carbonate deposits might function as bioseeds for calcium phosphate precipitation onto bone-forming cells.

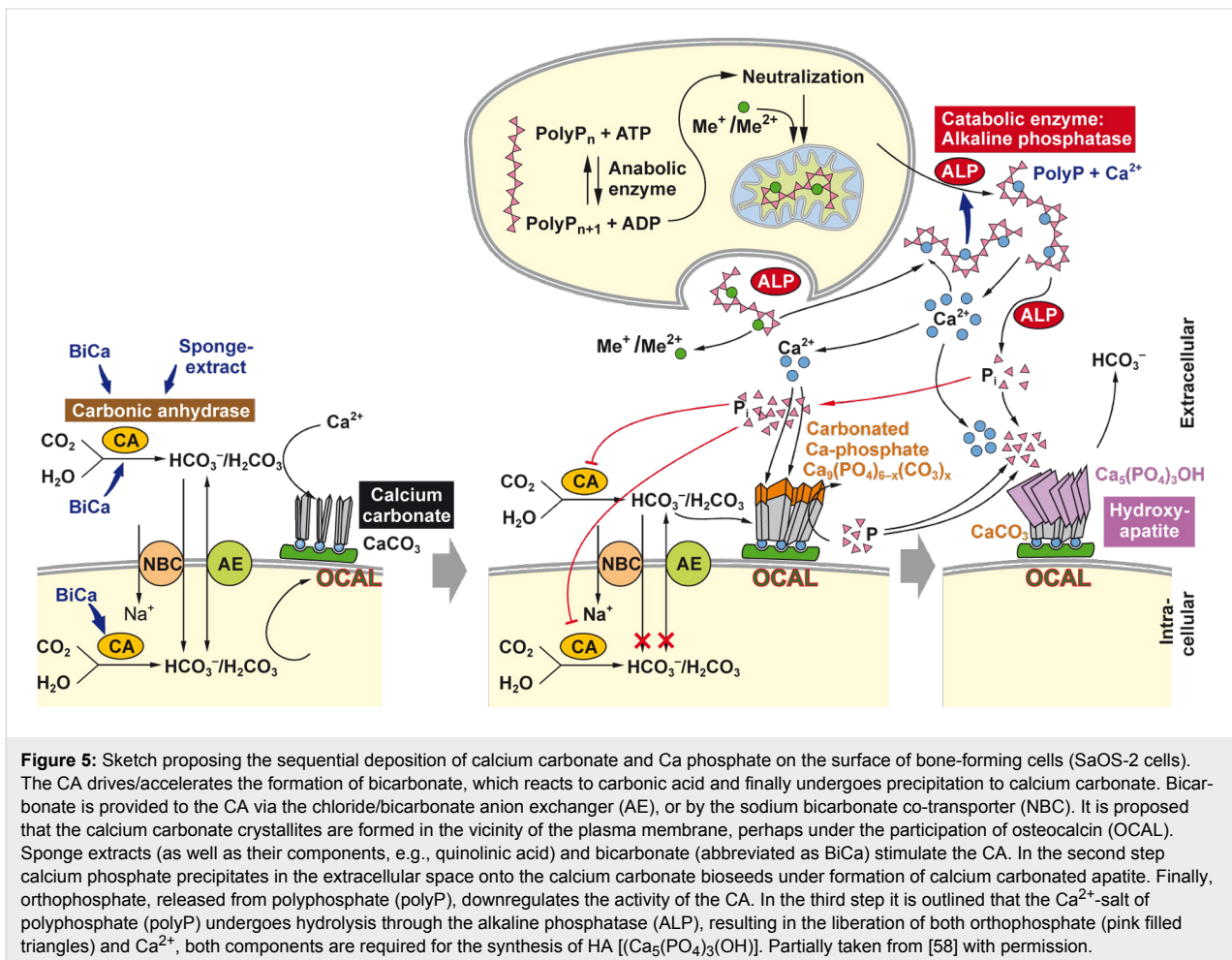
It is known that mineralization of osteoblasts, bone mineral-forming cells, is significantly induced by polyphosphate [polyP] in vitro even in the presence of orthophosphate [64]. PolyP is a linear polymer of phosphate linked by energy-rich phosphodiester bonds. Moreover, polyP turned out to be an inducer of osteoblast-specific alkaline phosphatase. This finding is interesting in view of published data indicating that intracellularly polyP might be formed in the vesicles of bone-forming cells as a Ca salt, which may act as a potential precursor of carbonated HA [65] (Figure 5).

In our recent study we could show that CA-driven  $\text{CaCO}_3$  deposition can be stimulated by CA activators in vitro [66]. As activator(s) we have chosen extracts from the sponge *S. domuncula* and one component, isolated from those extracts, quinolinic acid (QA). In the in vitro CA-driven calcium carbonate deposition assay we could demonstrate that the *S. domuncula* extract and QA stimulate mineral formation (Figure 3C); as controls, the assays had been performed in the absence of sponge extract or of pure QA. Furthermore the results revealed that the stimulatory effect of bicarbonate ions on mineralization onto osteoblast-like SaOS-2 cells is strongly enhanced if the cells are exposed to polyP [64]. Finally, after hydrolysis of polyP through the alkaline phosphatase, the liberated orthophosphate inhibits in a negative feedback circle the CA (Figure 5).

### Future direction: 3D printing

In the repair of critical-size bone defects, autogenous bone grafts are considered to be the gold standard [67]. This technique has, however, several limitations which cannot be solved by using allogeneous bone grafts, which have additional disadvantages, such as immunogenicity and risk of infection. Synthetic bone scaffolds can provide several advantages if they meet the following conditions: (i) similar physiochemical characteristics as the natural bone, and (ii) ability to attract the bone forming cells (the progenitor cells or the functionally active





differentiated cells), two challenging tasks, limiting the routine application of synthetic materials in the treatment of bone defects. Bone repair materials like calcium phosphate, calcium carbonate, calcium sulfate and coralline carbonate grafts are characterized by good mechanical properties. They can be used as osteoconductive implant materials. They also may show osteointegrative properties. However, these implants lack any osteoinductivity and must be functionalized to become biologically active (for a review, see [68]).

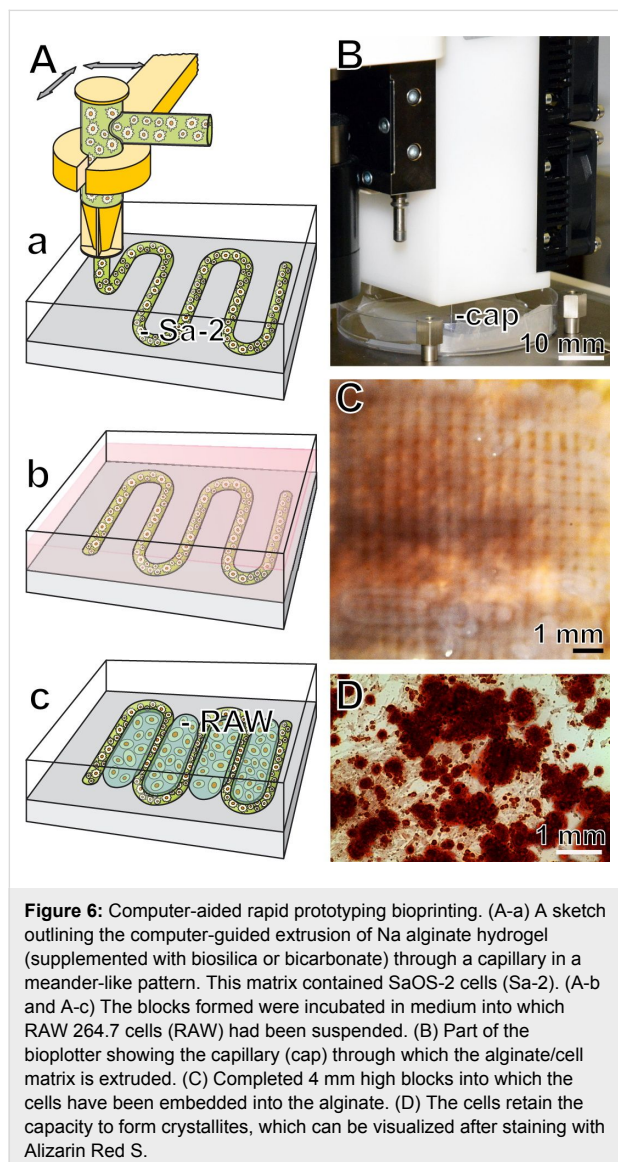
The prerequisite for any scaffold applicable for bone tissue engineering is that it is accepted by the cells as a suitable 3D platform for their growth, differentiation and mineralization (HA deposition). These requirements can be met by scaffolds made of natural fibers, which correspond in their structure and composition to the extracellular matrix. A suitable scaffold must possess the inorganic/organic 3D structure of bone and an appropriate porosity [69] that allows the ingrowth of cells and an efficient transport of cytokines, growth factors, and nutrients. To avoid necrosis within larger implants, a suitable scaffold must also allow an efficient vascularization and tissue supply

with oxygen. Much progress has been achieved in rapid prototyping/3D printing techniques in the last years. 3D printing is a computer-controlled layer-by-layer technology. Thereby a binder (binding solution) is printed into each layer of powder, a step-wise process that finally results, after blowing-away the unbound powder, in a 3D printed copy of the sliced virtual model [70,71]. 3D printing has turned out to be of promising technique for the fabrication of implants used as bone substitution materials [72]. The advantage of this method is that the implants can be customized to the 3D geometry of the bone defect of an individual patient, based on medical imaging data. Such implants allow an optimal integration and can be provided with the required functional properties using suitable materials such as bioactive glasses and Ca phosphate.

Based on published data, indicating that alginate/chitin, also together with silica [73,74], provides a suitable matrix for the encapsulation of mammalian cells we have recently also embedded SaOS-2 cells into Na alginate that has been supplemented with silica [75-77]. Silica displays morphogenetic activity towards SaOS-2 cells (see above); this biological

activity of silica is retained by SaOS-2 cells that have been encapsulated into Na alginate. Based on the finding that Na alginate is a suitable matrix for embedding bone cells [78] we have successfully started to print 3D structures in order to apply this technology for bioprinting and construction of bioartificial tissues or organs. In a first step we have encapsulated separately bone-forming (SaOS-2) and bone-degrading (RAW 264.7) cells to develop a biomimetic synthetic scaffold suitable for tissue engineering [75]. In the alginate matrix applied the SaOS-2 cells retain their capacity to synthesize HA crystallites. Furthermore, the mechanical properties, including surface roughness and hardness, of the hydrogel were determined. If silica is included in the hydrogel matrix, the encapsulated SaOS-2 cells were found to increasingly express the gene encoding for osteoprotegerin in co-cultivation experiments with RAW 264.7 cell beads, suggesting that under the applied condi-

tions the differentiation capacity of the RAW 264.7 cells is impaired. In continuation it was found that under these conditions (SaOS-2 cells cultured together with RAW 264.7 cells) the RAW 264.7 cells show a reduced capacity to express the gene for tartrate-resistant acid phosphatase. For rapid prototyping bioprinting we are using a computer-aided tissue engineering printer (3D-Bioplotter; Corporate EnvisionTEC GmbH, Gladbeck; Germany). With this technology we succeeded to embed SaOS-2 cells into the Na alginate, with the indicated supplements, and allowed the matrix to be passed through the capillary of the 3D printer (Figure 6). The arrays of strands were computed to 4 mm high blocks into which the cells remained viable and retained the capacity to form mineral crystallites. We are convinced that this strategy will contribute to a further improvement of the formulation of a suitable artificial scaffold for rapid prototyping 3D bioprinting of organ-like tissue units.



## Acknowledgements

W. E. G. M. is a holder of an ERC Advanced Investigator Grant (No. 268476 “BIOSILICA”) and of an ERC Proof-of-Concept Grant (No. 324564 “Si-Bone-PoC”). This work was supported by grants from the Deutsche Forschungsgemeinschaft (Schr 277/10-3), the European Commission (Industry-Academia Partnerships and Pathways “CoreShell”: No. 286059; “MarBioTec\*EU-CN\*”: No. 268476; “Bio-Scaffolds”: No. 604036; and “BlueGenics”: No. 311848) and the International Human Frontier Science Program, as well as the BiomaTiCS research initiative of the University Medical Center, Mainz.

## References

- Müller, W. E. G.; Wiens, M.; Adell, T.; Gamulin, V.; Schröder, H. C.; Müller, I. M. *Int. Rev. Cytol.* **2004**, *235*, 53–92. doi:10.1016/S0074-7696(04)35002-3
- Wang, X.; Schröder, H. C.; Müller, W. E. G. *Int. Rev. Cell Mol. Biol.* **2009**, *273*, 69–115. doi:10.1016/S1937-6448(08)01803-0
- Morse, D. E. *Trends Biotechnol.* **1999**, *17*, 230–232. doi:10.1016/S0167-7799(99)01309-8
- Wang, X.; Schröder, H. C.; Wang, K.; Kaandorp, J. A.; Müller, W. E. G. *Soft Matter* **2012**, *8*, 9501–9518. doi:10.1039/c2sm25889g
- Knoll, A. H. *Rev. Mineral. Geochem.* **2003**, *54*, 329–356. doi:10.2113/0540329
- Müller, W. E. G.; Li, J.; Schröder, H. C.; Qiao, L.; Wang, X. *Biogeosciences* **2007**, *4*, 219–232. doi:10.5194/bg-4-219-2007
- Müller, W. E. G.; Schröder, H. C.; Burghard, Z.; Pisignano, D.; Wang, X. *Chem.–Eur. J.* **2013**, *19*, 5790–5804. doi:10.1002/chem.201204412
- Müller, W. E. G. Spatial and temporal expression patterns in animals. In *Encyclopedia of Molecular Cell Biology and Molecular Medicine*; Meyers, R. A., Ed.; Wiley-VCH: Weinheim, Germany, 2005; Vol. 13, pp 269–309.
- Shimizu, K.; Cha, J.; Stucky, G. D.; Morse, D. E. *Proc. Natl. Acad. Sci. U. S. A.* **1998**, *95*, 6234–6238. doi:10.1073/pnas.95.11.6234

10. Cha, J. N.; Shimizu, K.; Zhou, Y.; Christianssen, S. C.; Chmelka, B. F.; Stucky, G. D.; Morse, D. E. *Proc. Natl. Acad. Sci. U. S. A.* **1999**, *96*, 361–365. doi:10.1073/pnas.96.2.361
11. Krasko, A.; Lorenz, B.; Batel, R.; Schröder, H. C.; Müller, I. M.; Müller, W. E. G. *Eur. J. Biochem.* **2000**, *267*, 4878–4887. doi:10.1046/j.1432-1327.2000.01547.x
12. Wiens, M.; Bausen, M.; Natalio, F.; Link, T.; Schlossmacher, U.; Müller, W. E. G. *Biomaterials* **2009**, *30*, 1648–1656. doi:10.1016/j.biomaterials.2008.12.021
13. Schloßmacher, U.; Wiens, M.; Schröder, H. C.; Wang, X.; Jochum, K. P.; Müller, W. E. G. *FEBS J.* **2011**, *278*, 1145–1155. doi:10.1111/j.1742-4658.2011.08040.x
14. Müller, W. E. G.; Binder, M.; von Lintig, J.; Guo, Y.-W.; Wang, X.; Kaandorp, J. A.; Wiens, M.; Schröder, H. C. *Biochim. Biophys. Acta, Gen. Subj.* **2011**, *1810*, 1178–1194. doi:10.1016/j.bbagen.2011.09.006
15. Wang, X.; Schloßmacher, U.; Schröder, H. C.; Müller, W. E. G. *Soft Matter* **2013**, *9*, 654–664. doi:10.1039/c2sm27109e
16. Wang, X.; Schröder, H. C.; Wiens, M.; Ushijima, H.; Müller, W. E. G. *Curr. Opin. Biotechnol.* **2012**, *23*, 570–578. doi:10.1016/j.copbio.2012.01.018
17. Katagiri, T.; Yamaguchi, A.; Komaki, M.; Abe, E.; Takahashi, N.; Ikeda, T.; Rosen, V.; Wozney, J. M.; Fujisawa-Sehara, A.; Suda, T. *J. Cell Biol.* **1994**, *127*, 1755–1766. doi:10.1083/jcb.127.6.1755
18. Mukherjee, A.; Rotwein, P. *J. Cell Sci.* **2009**, *122*, 716–726. doi:10.1242/jcs.042770
19. Heaney, R. P.; Recker, R. R.; Watson, P.; Lappe, J. M. *Am. J. Clin. Nutr.* **2010**, *92*, 101–105. doi:10.3945/ajcn.2009.29085
20. Müller, W. E. G.; Schröder, H. C.; Schlossmacher, U.; Grebenjuk, V. A.; Ushijima, H.; Wang, X. *Biomaterials* **2013**, *34*, 8671–8680. doi:10.1016/j.biomaterials.2013.07.096
21. Mann, S.; Parker, S. B.; Ross, M. D.; Skarnulis, A. J.; Williams, R. J. P. *Proc. R. Soc. London, Ser. B* **1983**, *218*, 415–424. doi:10.1098/rspb.1983.0048
22. Pisam, M.; Jammet, C.; Laurent, D. *Cell Tissue Res.* **2002**, *310*, 163–168. doi:10.1007/s00441-002-0622-z
23. Pellegrino, E. D.; Biltz, R. M. *Calcif. Tissue Res.* **1970**, *6*, 168–171. doi:10.1007/BF02196196
24. Azari, F.; Vali, H.; Guerin-Kern, J.-L.; Wu, T.-D.; Croisy, A.; Sears, S. K.; Tabrizian, M.; McKee, M. D. *J. Struct. Biol.* **2008**, *162*, 468–479. doi:10.1016/j.jsb.2008.03.003
25. Rey, C.; Kim, H.-M.; Gerstenfeld, L.; Glimcher, M. J. *Connect. Tissue Res.* **1996**, *35*, 343–349. doi:10.3109/03008209609029210
26. Boonrungsiman, S.; Gentleman, E.; Carzaniga, R.; Evans, N. D.; McComb, D. W.; Porter, A. E.; Stevens, M. M. *Proc. Natl. Acad. Sci. U. S. A.* **2012**, *109*, 14170–14175. doi:10.1073/pnas.1208916109
27. Omelon, S.; Georgiou, J.; Henneman, Z. J.; Wise, L. M.; Sukhu, B.; Hunt, T.; Wynnyckyj, C.; Holmyard, D.; Bielecki, R.; Grynepas, M. D. *PLoS One* **2009**, *4*, e5634. doi:10.1371/journal.pone.0005634
28. Posner, A. S.; Betts, F.; Blumenthal, N. C. *Metab. Bone Dis. Relat. Res.* **1978**, *1*, 179–183. doi:10.1016/0221-8747(78)90057-7
29. Li, W.; Chen, W.-S.; Zhou, P.-P.; Cao, L.; Yu, L.-J. *Colloids Surf., B* **2013**, *102*, 281–287. doi:10.1016/j.colsurfb.2012.08.042
30. Meldrum, F. C.; Cölfen, H. *Chem. Rev.* **2008**, *108*, 4332–4432. doi:10.1021/cr8002856
31. Müller, W. E. G.; Schröder, H. C.; Schlossmacher, U.; Neufurth, M.; Geurtsen, W.; Korzhev, M.; Wang, X. *FEBS Open Bio* **2013**, *3*, 357–362. doi:10.1016/j.fob.2013.08.004
32. Lindskog, S. *Pharmacol. Ther.* **1997**, *74*, 1–20. doi:10.1016/S0163-7258(96)00198-2
33. Sanyal, G.; Maren, T. H. *J. Biol. Chem.* **1981**, *256*, 608–612.
34. Sly, W. S.; Hu, P. Y. *Annu. Rev. Biochem.* **1995**, *64*, 375–401. doi:10.1146/annurev.bi.64.070195.002111
35. Chang, X.; Zheng, Y.; Yang, Q.; Wang, L.; Pan, J.; Xia, Y.; Yan, X.; Han, J. *Arthritis Res. Ther.* **2012**, *14*, R176. doi:10.1186/ar3929
36. Alvarez, L.; Fanjul, M.; Carter, N.; Hollande, E. *J. Histochem. Cytochem.* **2001**, *49*, 1045–1053. doi:10.1177/002215540104900812
37. Mahieu, I.; Becq, F.; Wolfensberger, T.; Gola, M.; Carter, N.; Hollande, E. *Biol. Cell* **1994**, *81*, 131–141. doi:10.1016/S0248-4900(94)80004-9
38. Müller, W. E. G.; Wang, X.; Grebenjuk, V. A.; Korzhev, M.; Wiens, M.; Schloßmacher, U.; Schröder, H. C. *PLoS One* **2012**, *7*, e34617. doi:10.1371/journal.pone.0034617
39. Lovejoy, D. A.; Hewett-Emmett, D.; Porter, C. A.; Cepoi, D.; Sheffield, A.; Vale, W. W.; Tashian, R. E. *Genomics* **1998**, *54*, 484–493. doi:10.1006/geno.1998.5585
40. Furla, P.; Galgani, I.; Durand, I.; Allemand, D. *J. Exp. Biol.* **2000**, *203*, 3445–3457.
41. Tripp, B. C.; Smith, K.; Ferry, J. G. *J. Biol. Chem.* **2001**, *276*, 48615–48618. doi:10.1074/jbc.R100045200
42. Müller, W. E. G.; Schlossmacher, U.; Schröder, H. C.; Lieberwirth, I.; Glasser, G.; Korzhev, M.; Neufurth, M.; Wang, X. *Acta Biomater.* **2014**, *10*, 450–462. doi:10.1016/j.actbio.2013.08.025
43. Jones, W. C. *Nature* **1967**, *214*, 365–368. doi:10.1038/214365a0
44. Ledger, P. W.; Jones, W. C. *Cell Tissue Res.* **1977**, *181*, 553–567. doi:10.1007/BF00221776
45. Han, T. Y.-J.; Aizenberg, J. *Chem. Mater.* **2008**, *20*, 1064–1068. doi:10.1021/cm702032v
46. Tyrrell, T. *J. Plankton Res.* **2008**, *30*, 141–156. doi:10.1093/plankt/fbm105
47. Gasbjerg, P. K.; Brahm, J. *J. Gen. Physiol.* **1991**, *97*, 321–349. doi:10.1085/jgp.97.2.321
48. Li, W.; Chen, W.-S.; Zhou, P.-P.; Zhu, S.-L.; Yu, L.-J. *Chem. Eng. J.* **2013**, *218*, 65–72. doi:10.1016/j.cej.2012.12.034
49. Ilan, M.; Aizenberg, J.; Gilor, O. *Proc. R. Soc. London, Ser. B* **1996**, *263*, 133–139. doi:10.1098/rspb.1996.0021
50. Müller, W. E. G.; Neufurth, M.; Schlossmacher, U.; Schröder, H. C.; Pisignano, D.; Wang, X. *RSC Adv.* **2014**, *4*, 2577–2585. doi:10.1039/c3ra45193c
51. Kirley, J. W.; Day, R. A. *Biochem. Biophys. Res. Commun.* **1985**, *126*, 457–463. doi:10.1016/0006-291X(85)90627-8
52. Margolis, D. S.; Szivek, J. A.; Lai, L.-W.; Lien, Y.-H. H. *Calcif. Tissue Int.* **2008**, *82*, 66–76. doi:10.1007/s00223-007-9098-x
53. Müller, W. E. G.; Müller, I.; Zahn, R. K.; Maidhof, A. *J. Histochem. Cytochem.* **1984**, *32*, 285–288. doi:10.1177/32.3.6141203
54. Termine, J. D.; Eanes, E. D.; Greenfield, D. J.; Nysten, M. U.; Harper, R. A. *Calcif. Tissue Res.* **1973**, *12*, 73–90. doi:10.1007/BF02013723
55. Biltz, R. M.; Pellegrino, E. D. *Clin. Orthop. Relat. Res.* **1977**, *129*, 279–292.
56. Matsuura, A.; Kubo, T.; Doi, K.; Hayashi, K.; Morita, K.; Yokota, R.; Hayashi, H.; Hirata, I.; Okazaki, M.; Akagawa, Y. *Dent. Mater. J.* **2009**, *28*, 234–242. doi:10.4012/dmj.28.234

57. Novak, I.; Greger, R. *Pfluegers Arch.* **1988**, *411*, 546–553. doi:10.1007/BF00582376
58. Wang, X.; Schröder, H. C.; Feng, Q.; Draenert, F.; Müller, W. E. G. *Mar. Drugs* **2013**, *11*, 718–746. doi:10.3390/md11030718
59. Garrett, I. R. *Curr. Top. Dev. Biol.* **2007**, *78*, 127–171. doi:10.1016/S0070-2153(06)78004-8
60. Supuran, C. T.; Scozzafava, A. *Expert Opin. Ther. Pat.* **2000**, *10*, 575–600. doi:10.1517/13543776.10.5.575
61. Pastorekova, S.; Parkkila, S.; Pastorek, J.; Supuran, C. T. *J. Enzyme Inhib. Med. Chem.* **2004**, *19*, 199–229. doi:10.1080/14756360410001689540
62. Supuran, C. T. *Nat. Rev. Drug Discovery* **2008**, *7*, 168–181. doi:10.1038/nrd2467
63. Supuran, C. T. *Curr. Pharm. Des.* **2008**, *14*, 603–614. doi:10.2174/138161208783877884
64. Müller, W. E. G.; Wang, X.; Diehl-Seifert, B.; Kropf, K.; Schloßmacher, U.; Lieberwirth, I.; Glasser, G.; Wiens, M.; Schröder, H. C. *Acta Biomater.* **2011**, *7*, 2661–2671. doi:10.1016/j.actbio.2011.03.007
65. Mahamid, J.; Sharir, A.; Gur, D.; Zelzer, E.; Addadi, L.; Weiner, S. *J. Struct. Biol.* **2011**, *174*, 527–535. doi:10.1016/j.jsb.2011.03.014
66. Wang, X.; Schröder, H. C.; Schlossmacher, U.; Neufurth, M.; Feng, Q.; Diehl-Seifert, B.; Müller, W. E. G. *Calcif. Tissue Int.* **2014**, *94*, 495–509. doi:10.1007/s00223-013-9833-4
67. Epple, M. Biomimetic Bone Substitution Materials. In *Biomimetic Bone Substitution Materials. In Biomimetic Bone Substitution Materials. Medical and Clinical Aspects*; Epple, M.; Baeuerlein, E., Eds.; Wiley-VCH: Weinheim, Germany, 2007; pp 81–95.
68. Brydone, A. S.; Meek, D.; MacLaine, S. *J. Eng. Med.* **2010**, *224*, 1329–1343. doi:10.1243/09544119JEIM770
69. Holzwarth, J. M.; Ma, P. X. *Biomaterials* **2011**, *32*, 9622–9629. doi:10.1016/j.biomaterials.2011.09.009
70. Seitz, H.; Rieder, W.; Irsen, S.; Leukers, B.; Tille, C. *J. Biomed. Mater. Res., Part B* **2005**, *74*, 782–788. doi:10.1002/jbm.b.30291
71. Fierz, F. C.; Beckmann, F.; Huser, M.; Irsen, S. H.; Leukers, B.; Witte, F.; Degistirici, Ö.; Andronache, A.; Thie, M.; Müller, B. *Biomaterials* **2008**, *29*, 3799–3806. doi:10.1016/j.biomaterials.2008.06.012
72. Detsch, R.; Schaefer, S.; Deisinger, U.; Ziegler, G.; Seitz, H.; Leukers, B. *J. Biomater. Appl.* **2011**, *26*, 359–380. doi:10.1177/0885328210373285
73. Gimeno-Fabra, M.; Peroglio, M.; Eglin, D.; Alini, M.; Perry, C. C. *J. Mater. Chem.* **2011**, *21*, 4086–4089. doi:10.1039/c0jm04463f
74. Madhumathi, K.; Sudheesh Kumar, P. T.; Kavya, K. C.; Furuike, T.; Tamura, H.; Nair, S. V.; Jayakumar, R. *Int. J. Biol. Macromol.* **2009**, *45*, 289–292. doi:10.1016/j.ijbiomac.2009.06.009
75. Schloßmacher, U.; Schröder, H. C.; Wang, X.; Feng, Q.; Diehl-Seifert, B.; Neumann, S.; Trautwein, A.; Müller, W. E. G. *RSC Adv.* **2013**, *3*, 11185–11194. doi:10.1039/c3ra23341c
76. Müller, W. E. G.; Wang, X.; Grebenjuk, V.; Diehl-Seifert, B.; Steffen, R.; Schloßmacher, U.; Trautwein, A.; Neumann, S.; Schröder, H. C. *Biomater. Sci.* **2013**, *1*, 669–678. doi:10.1039/c3bm00001j
77. Wang, X.; Schröder, H. C.; Diehl-Seifert, B.; Kropf, K.; Schlossmacher, U.; Wiens, M.; Müller, W. E. G. *J. Tissue Eng. Regen. Med.* **2013**, *7*, 767–776. doi:10.1002/term.1465
78. Song, S.-J.; Choi, J.; Park, Y.-D.; Hong, S.; Lee, J. J.; Ahn, C. B.; Choi, H.; Sun, K. *Artif. Organs* **2011**, *35*, 1132–1136. doi:10.1111/j.1525-1594.2011.01377.x

## License and Terms

This is an Open Access article under the terms of the Creative Commons Attribution License (<http://creativecommons.org/licenses/by/2.0>), which permits unrestricted use, distribution, and reproduction in any medium, provided the original work is properly cited.

The license is subject to the *Beilstein Journal of Nanotechnology* terms and conditions: (<http://www.beilstein-journals.org/bjnano>)

The definitive version of this article is the electronic one which can be found at: doi:10.3762/bjnano.5.72